



Olive-stone biomass ash (OBA): An alternative alkaline source for the blast furnace slag activation

Sayonara Maria de Moraes Pinheiro^a, Alba Font^b, Lourdes Soriano^b, Mauro M. Tashima^c, José Monzó^b, Maria Victoria Borrachero^b, Jordi Payá^{b,*}

^aUFES – Federal University of Espírito Santo, Department of Civil Engineering, Brazil

^bICITECH – GIQUIMA Group – Grupo de Investigación en Química de los Materiales de Construcción, Instituto de Ciencia y Tecnología del Hormigón, Universitat Politècnica de Valencia, Valencia, Spain

^cUNESP – Grupo de Pesquisa MAC – Materiais Alternativos de Construção, Universidade Estadual Paulista, Campus de Ilha Solteira, São Paulo, Brazil

HIGHLIGHTS

- Olive-stone biomass ash (OBA) was successfully tested as activator.
- OBA has alkaline properties suitable for alkali activated materials (AAM).
- OBA was used as unique activator for blast furnace slag (BFS).
- The effectivity of OBA was higher than KOH and similar to NaOH.
- OBA reduces the consumption of commercial chemical reagents in AAM.

ARTICLE INFO

Article history:

Received 28 February 2018

Received in revised form 24 April 2018

Accepted 19 May 2018

Available online 26 May 2018

Keywords:

Conservation

Alkali activated material

Blast furnace slag

Olive-stone biomass ash

Strength development

ABSTRACT

Alkali activated materials (AAM) are being investigated as an alternative binder that could be more eco-efficient than Portland cement. The effect of olive-stone biomass ash (OBA) on the activation of blast furnace slag (BFS) was studied. The mechanical behaviour of mortars in which OBA was replaced, or added to, BFS were compared to those found for BFS mortars activated with potassium hydroxide (KOH) and sodium hydroxide (NaOH) solutions in the range of 4–12 mol·kg⁻¹. The results showed the high efficiency of OBA as activating reagent because it provided similar, or higher, strengths when compared to the alkali hydroxide activating solutions. The microstructural characteristics of the new binding OBA/BFS systems were assessed by X-ray diffraction (XRD), thermogravimetric analysis (TGA), field emission scanning electron microscopy (FESEM) and mercury intrusion porosimetry (MIP). These systems showed lower mean pore diameter and scarcer formation of zeolite structures when compared to KOH/BFS systems. These promising results demonstrated the viability of the use of these type of ashes as activating reagents in AAM.

© 2018 Elsevier Ltd. All rights reserved.

1. Introduction

Currently, cementing materials resulting from alkaline activation of alumino-silicate precursors are becoming a well-known alternative to Portland cement. They are overcoming the limitations of Portland cement in terms of mechanical and durability performance, and also minimize environmental impacts, such as CO₂ emissions and energy consumption [1]. These materials are denominated as alkali-activated materials (AAM) or geopolymers [2–4].

In general, the raw materials used as source of alumino-silicates are blast furnace slag (BFS) [5,6], metakaolin [7] or fly ash [8,9]. In the last few years, some industrial and agricultural wastes have been investigated, and some of them have shown the ability for alkali-activated procedures in simple or combined systems, such as fluid catalytic cracking catalyst FCC residue [10], ceramic waste [11,12], bottom coal ash [13] and sugarcane waste-derived ash [14], among others.

However, there are fewer examples in which wastes have been used in the preparation of the activating solution. This is a critical subject, because the environmental impact relates to its synthesis. The commercial reagents for preparing solutions used to activate the precursor are produced with natural raw materials and involve

* Corresponding author.

E-mail address: jjpaya@cst.upv.es (J. Payá).

industrial processes with high energy costs and high CO₂ emission, especially the alkali silicates [15,16].

In order to minimize this impact, several studies have been done [15–20]. Gao et al. [15] reported the use of nanosilica from olivine for preparing alkali activating reagents for the activation of slag-fly ash blends. In some cases, the goal was to supply soluble silicate by dissolution of the rice husk ash [16–20]. The reagent for producing the dissolution was commercial sodium hydroxide, and the results indicated the feasibility of its use. However, very few studies were reported in which AAM was prepared with raw materials (precursor and activating solution) and were derived exclusively from waste (100%-waste AAM).

Recently, an alkaline sodium hydroxide waste solution from an aluminium cleaning mould process was studied [21]. In this study, the waste was used to supply the alkali activating solution on different precursors, and the results were promising for its use in the industry of geopolymers.

In this context, olive-stone biomass ash (OBA) comes up as a promising alkali source for preparation of AAMs. It has a significant amount of potassium and when mixed with BFS, showed promising properties, such as compressive and flexural strengths of the mortar [22]. Also, ashes from maize stalk and maize cob were used for activating metakaolin [23].

During the production of olive oil, two types of waste are generated, a liquid (waste water) and a solid phase (Fig. 1). The liquid phase, “alpechín” (wastewater from olive oil mills), contains a large number of solid residues, oil, grease and polyphenols. It is a highly contaminant material [24–27] because of its acidity and high chemical (DQO) and biochemical (DQO) oxygen demands. The solid waste (SW) phase is a paste formed by a mixture of pulp, bark, olive stone and residual oil, called “orujo”, “alpeorujo”, “orujillo” or “cake”. This SW has a high concentration of organic matter, oil and grease, and is rich in calcium and potassium [28–30]. It is a contaminant material, has a strong smell and high moisture content. It can be used as an energy resource, such as for biofuel, animal feed and soil fertilizer [24,31,32].

The amount of the SW and its physical-chemical characteristics depend on the production process used for the oil extraction. It has been estimated that in 1000 kg of olive oil production, 1500–4000 kg of SW are generated. In addition to the type of process, changes in yield and contamination of the waste can occur [29,30,32,33].

The world production of olive oil expected for 2016/2017 is estimated to be 2.7 Mt, and 92% will be produced in the Mediterranean area and 48.3% in Spain [34]. Considering the average residue generation rate, where solid waste/olive oil = 2.5, it is possible to expect the generation of 4.9 Mt of SW in Spain.

To be used as a biofuel, the SW must be dried. In addition, the stone can be segregated to generate a by-product with a higher calorific value about 4490 kcal/kg [35]. The combustion of these solid waste phases generates ashes (Fig. 1): a general olive waste ash (OWA) and a specific olive-stone biomass ash (OBA) [25]. The chemical characteristics of these ashes depend on many factors, such as SW composition, combustion temperature and the presence of contaminants (Table 1). The estimated amount of ash generated in the burning process from dried SW is about 12% by mass [36].

The reuse of these ashes in the preparation of concrete and mortars has been widely reported [36–39]. The studies with OWA were done with concrete and mortars, using it as a replacement material for Portland cement, fine filler material and sand [36–39].

Specifically, Eisa [39] found a reduction in the compressive and flexural strengths of concrete when OWA was used as a replacement for Portland cement. Al-Akhras et al. [36], obtained a more durable material at high temperatures when OWA was used as a replacement for Portland cement. It was also more resistant to the alkali-silica reaction, when OWA was used as a replacement for sand [38]. The authors explained the improvement in the performance of the material due to a possible pozzolanic and filler effects of OWA.

Al-Akhras and Abdulwahid [37] used OWA as a replacement for Portland cement and sand in mortars. The mortars they produced showed a decrease in the workability with the increase of OWA

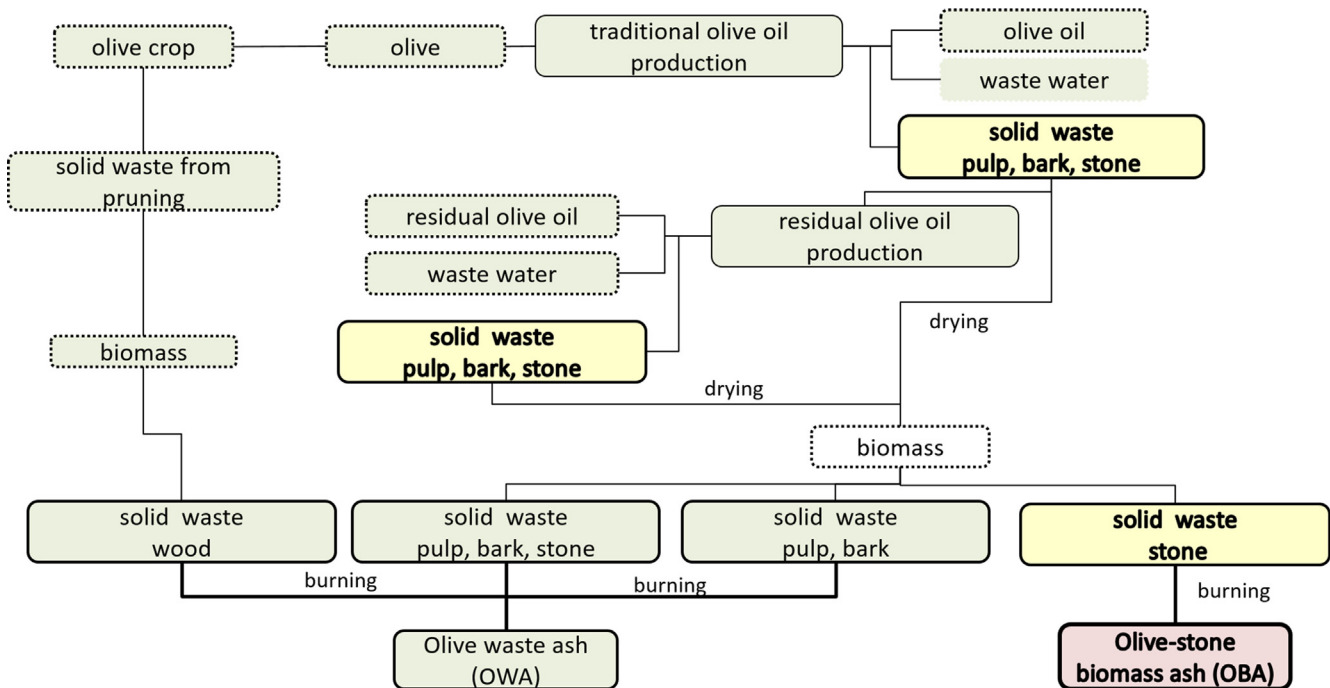


Fig. 1. Scheme of the production of olive oils, generation of wastes and their ashes by combustion.

Table 1
Reported chemical compositions for OWA and OBA.

Waste	SiO ₂	CaO	Al ₂ O ₃	Fe ₂ O ₃	Na ₂ O	K ₂ O	MgO	P ₂ O ₅	SO ₃	LOI	REF
OWA – wood	2.70	52.30	1.40	2.10	0.10	1.50	2.70	1.50	2.60	32.06	[35]
	8.10	32.80	1.60	0.70	2.90	19.90	2.40	8.50	2.10	20.90	[35]
	9.20	43.40	1.50	1.90	2.70	12.70	2.80	12.70	1.70	11.20	[35]
	10.00	44.20	1.20	1.00	2.60	7.20	3.50	17.00	6.80	6.40	[35]
	10.24	41.47	2.02	0.88	3.67	25.16	3.03	10.75	2.65	–	[41]
	11.84	54.82	2.60	1.38	0.16	9.26	4.36	3.40	–	11.73	[42]
OWA – bark	32.70	14.50	8.40	6.30	26.20	4.30	4.20	2.50	0.60	–	[43]
OWA – pulp, bark and stone	22.26	12.93	4.10	1.99	0.12	42.79	5.84	6.09	3.73	–	[41]
	33.00	18.14	16.66	6.50	2.50	11.20	10.00	–	2.93	3.52	[40]
OWA – pulp and bark	25.30	42.40	7.40	4.60	0.45	3.30	3.20	–	3.70	9.50	[36]
	25.80	42.90	8.50	5.70	0.25	0.33	3.20	–	3.80	9.50	[37]
	25.80	42.90	8.50	5.70	0.25	0.33	3.20	–	3.80	9.50	[38]
	31.47	13.66	6.45	6.97	27.43	1.77	4.48	33.33	1.98	–	[44]
OBA – stone	21.40	33.00	4.40	7.90	0.60	2.70	3.70	2.30	4.40	18.70	[35]
	10.70	22.00	2.70	1.70	3.40	24.70	3.00	14.70	3.50	13.30	[35]
	15.00	28.70	3.10	2.30	4.10	19.90	4.20	11.60	2.50	8.30	[35]
	20.40	32.90	4.40	2.60	4.30	12.70	4.80	11.10	4.80	1.50	[35]
	21.48	19.97	5.95	4.25	15.77	16.44	3.84	9.71	2.30	–	[41]
	5.33	27.77	0.70	3.45	0.78	32.12	5.13	2.68	1.67	18.90	[22]

content. Also, they observed an increase in the compressive and flexural strengths when sand was replaced with OWA, and a decrease when Portland cement was replaced by it. Cruz-Yusta et al. [40] analysed the effect of OWA as a replacement for Portland cement and as a filler material. The authors concluded that a replacement of up to 10% of Portland cement is feasible without major changes in strength, and showed a low pozzolanic activity of the material, as well as its filler effect.

The first study of OBA was carried out by Font et al. [22]. The ash was characterized and it showed a high amount of K₂O (32.16%) and CaO (27.77%). They also noted the high alkalinity in water suspension (pH = 13.5) and the presence of crystalline phases, such as portlandite, calcite, anorthite and kalicinite. These characteristics show that the material can be a potential source of alkalis in AAMs. In this first study, the potential of OBA in alkaline activation was assessed in BFS mortars and three types of mixtures (BFS/water, BFS/KOH and BFS/OBA). The results showed: a) the BFS was alkali activated by the OBA, b) the AAM matrix produced with OBA was stronger than the matrix produced with KOH and c) a filler effect in the matrix was observed.

To better understand of the behaviour of OBA in AAM, this study analysed the binary system composed by blast furnace slag (BFS) and olive-stone biomass ash (OBA) to evaluate the alkaline reactive potential of OBA. A comparison in mechanical behaviour and microstructural parameters was carried out in order to assess the role of OBA, and the effect of the percentage of OBA, in the prepared BFS-based mixtures.

2 Materials and methods

2.1. Materials

The materials used in this experiment were blast furnace slag (BFS), olive-stone biomass ash (OBA), kephalite (KPH), potassium hydroxide (KOH) and sodium hydroxide (NaOH).

Blast furnace slag (BFS) was used as a precursor in all mixtures. It was supplied by Cementval (Puerto de Sagunto, Valencia, Spain). The particle size distribution is shown in Fig. 2. It had 26.0 μm mean particle diameter and its chemical composition is summarized in Table 2.

Olive-stone biomass ash (OBA) was supplied by Almazara Candela – Elche, Spain. It was produced in the combustion of olive-stone to produce heat. The resulting ash was collected from the bottom of the furnace. The received sample was dried at 105 °C

for 24 h and was immediately ground into a ball mill in order to homogenize the material, increase its fineness and improve its dissolution rate in water. It presented 27.4 μm mean particle diameter, and the particle size distribution is shown in Fig. 2. Its chemical composition is summarized in Table 2. The XRD pattern showed the main crystalline phases (Fig. 3) as portlandite (Ca(OH)₂, PDF card 040733), calcite (CaCO₃, PDF card 050586), anorthite (CaAl₂Si₂O₈, PDF card 411486) and kalicinite (KHCO₃, PDF card 120292). Also, quartz (SiO₂, PDF card 331161), silvite (KCl, PDF card 411476) and gismondine (CaAl₂Si₂O₈·4H₂O, PDF card 200452) were detected. The size and shape of ground OBA particles are depicted in Fig. 4. In general, OBA particles were porous and irregular, and some particles presented a smooth surface (these were identified as unburned olive-stone particles).

Kephalite (KPH) is a pure crystalline andalucite (Al₂SiO₅, 63% in Al₂O₃ and 37% in SiO₂ by weight) which is used as inert material because of its low solubility in an alkaline medium (the solubility in boiling 4 M KOH solution for 4 h was less than 5%). The particle size distribution is shown in Fig. 2, and its mean particle diameter was 31.1 μm.

Commercial potassium hydroxide (KOH, 85% purity, pellets) and sodium hydroxide (NaOH, 98% purity, pellets) were supplied by Panreac S.A.

2.2. Methods

The methodology applied to evaluate the reactive potential of OBA, as an alkaline source to activate BFS, included the analysis of mechanical properties and microstructural characteristics obtained in mortars and pastes. Alkali activated samples were produced with different mass ratios of BFS/OBA. The control mortars and pastes were produced with BFS/KOH, BFS/NaOH and BFS/KOH + KPH.

Mortars were prepared with w/b = 0.4 (water/binder, being the binder the quantity of BFS in control mortars) and a/b = 3 (aggregate/binder) ratios. The fresh mixture was poured in three prismatic 40 × 40 × 160 mm³ moulds and they were demoulded after 4 h in a thermal bath (65 °C). The specimens were cured for 7 days at 65 °C. Three values for flexural strength (Rf) and six values for compressive strength (Rc) were obtained for each mixture according to UNE 196-1 [45].

Alkaline activation of BFS was assessed by a family of mortars produced with BFS/KOH and BFS/NaOH in different concentrations. These mortars were noted as BFS/KOH-xM and BFS/NaOH-xM,

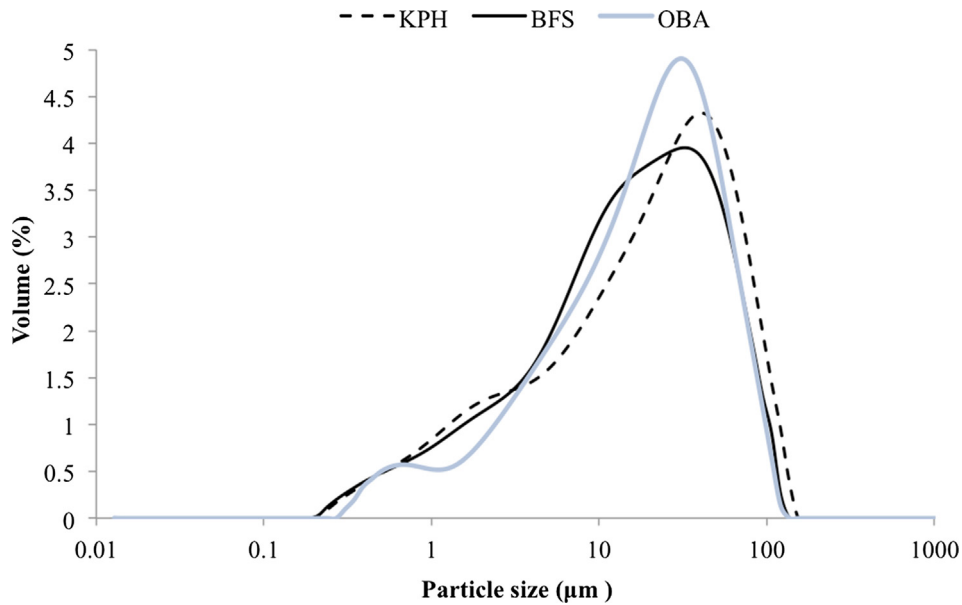


Fig. 2. Particle size distribution curves for BFS, OBA and KPH.

Table 2
Chemical compositions for BFS and OBA.

Materials	Oxide composition (%)										
	SiO ₂	CaO	Al ₂ O ₃	Fe ₂ O ₃	Na ₂ O	MgO	K ₂ O	P ₂ O ₅	SO ₃	others	LOI
BFS	30.53	40.15	10.55	1.29	0.87	7.43	0.57	0.26	1.93	0.89	5.53
OBA	5.33	27.77	0.70	3.45	0.78	5.13	32.12	2.68	1.67	0.95	18.90

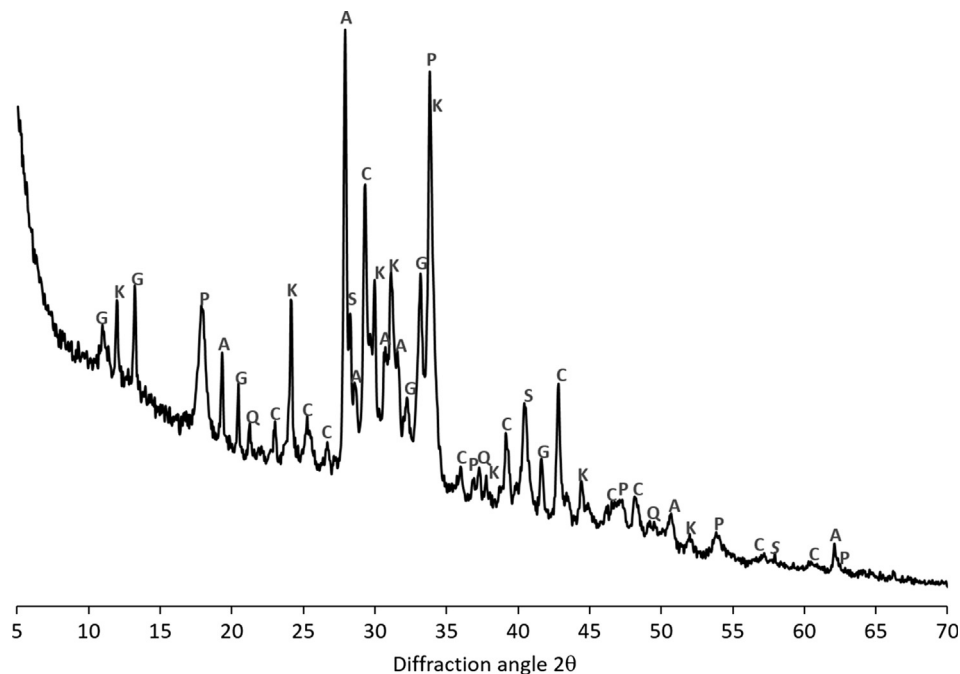


Fig. 3. X-ray diffraction pattern of OBA (Key: P, portlandite; C, calcite; A, anorthite; K, kalinicite; Q, quartz; S, silvite; G, gismondine).

where “x” is the molality ($\text{mol}\cdot\text{kg}^{-1}$) value of the alkaline solution ($x = 4, 6, 8, 10, 12$ and $14 \text{ mol}\cdot\text{kg}^{-1}$; the symbol M will be used in the manuscript for simplicity).

The filler effect was controlled by means of mortars produced with BFS/KOH + KPH. Two types of mortars with 4 M KOH were

synthesized, one with KPH 20% addition (Ad) respect to BFS and the other with 20% replacement (Rp) of the BFS. They were named as KPH-Ad20-4M and KPH-Rp20-4M, respectively.

BFS/OBA mortars were produced by blending both solids. An addition series (Ad) was prepared, where a given percentage of

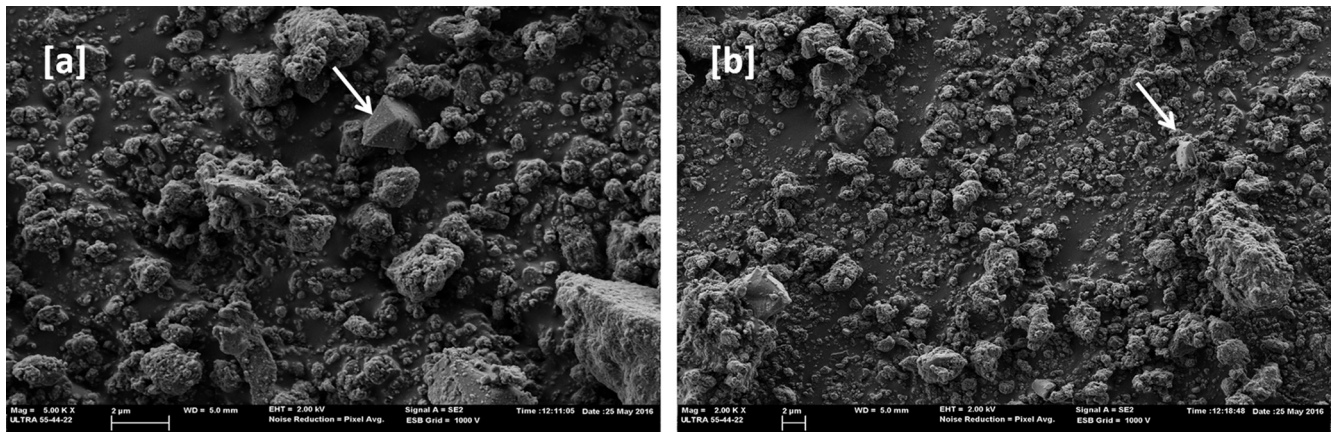


Fig. 4. FESEM micrographs for OBA: a) 5000 \times ; b) 2000 \times . Arrows indicate the presence of unburned olive-stone particles.

OBA was added by mass with respect to BFS content, and a replacement series (Rp) was prepared by the substitution by mass of BFS by OBA. They were named as OBA-Ady and OBA-Rpz respectively, where “y” is the addition content of OBA ($y = 5, 10, 15, 20$ and 25%) and “z” is the replacement by OBA ($z = 15, 20, 25, 30$ and 35%).

The pastes used in these analyses were prepared with $w/b = 0.4$ and were moulded in a plastic container, sealed and cured for 7 days at 65°C . The microstructure of the hydrated products in the pastes was evaluated by: a) powder X-ray diffraction (XRD), carried out by a Bruker AXS D8 Advance, from 10° to $70^\circ 2\theta$, and with $\text{Cu K}\alpha$ radiation at 40 kV and 20 mA ; b) thermogravimetric analysis (TG/DTG), using a TGA850 Mettler Toledo thermobalance with a temperature range of $35\text{--}600^\circ\text{C}$, heating rate of $10^\circ\text{C min}^{-1}$ in an N_2 atmosphere with $75\text{ mL}\cdot\text{min}^{-1}$ gas flow; c) field emission scanning electron microscopy (FESEM) by an ULTRA 55-ZEISS (the powdered sample of OBA was not covered by any material and the pastes were covered by carbon) and EDS with $6\text{--}8\text{ mm}$ work distance and extra high voltage of 20 kV ; and d) mercury intrusion porosimetry (MIP) by means of an AutoPore IV 9500 by the Micromeritics Instrument Corporation, that measured pores in the range of $91.26\text{ }\mu\text{m}\text{--}5.5\text{ nm}$.

For TG/DTG and XRD, 5 types of pastes were analysed: P-BFS/KOH- $x\text{M}$ ($x = 4$ and 8 M), P-OBA-Ad x ($x = 20$ and 25%) and P-KPH-Ad20-4M. For FESEM and porosity studies, 4 types of pastes were analysed: P-BFS/KOH- $x\text{M}$ ($x = 4, 8\text{ M}$) and P-OBA-Ad x ($x = 10$ and 25%).

3. Results and discussion

3.1. BFS activated by KOH and NaOH

The effect of KOH and NaOH solutions on the hydration of BFS was evaluated by the mechanical and microstructural performance of mortars and pastes. Samples were prepared by means of alkali activating solutions with different concentrations of KOH and NaOH. The mechanical properties evaluated in mortars included the compressive (R_c) and flexural (R_f) strengths. In Table 3, the mechanical properties are summarized, while in Figs. 5 and 6 a comparison of the compressive and flexural strengths of the mortars is shown respectively.

The KOH series showed a nonlinear behaviour with alkali concentration and a maximum R_c value was found for [KOH] equal to 8 M . For this mixture, the R_c value reached 25.56 MPa . The lowest values were found for [KOH] equal to 4 M and 14 M (in the $14\text{--}15\text{ MPa}$ range), whereas R_c values in the range $19\text{--}21\text{ MPa}$ were obtained for the rest of the KOH mortars. A similar trend

Table 3

Mechanical properties (compressive, R_c ; flexural, R_f) of mortars cured for 7 days at 65°C .

Mortars	Mechanical properties	
	R_c (MPa)	R_f (MPa)
BFS/KOH-4M	14.55 ± 0.70	3.38 ± 0.15
BFS/KOH-6M	20.31 ± 0.32	3.90 ± 0.02
BFS/KOH-8M	25.56 ± 0.73	3.73 ± 0.53
BFS/KOH-10M	20.77 ± 0.64	2.32 ± 0.18
BFS/KOH-12M	19.31 ± 0.67	2.35 ± 0.14
BFS/KOH-14M	14.94 ± 0.66	1.79 ± 0.07
BFS/NaOH-4M	17.57 ± 0.59	3.95 ± 0.34
BFS/NaOH-6M	24.07 ± 0.38	5.64 ± 0.25
BFS/NaOH-8M	26.90 ± 0.67	5.82 ± 0.71
BFS/NaOH-10M	27.90 ± 0.64	4.35 ± 0.36
BFS/NaOH-12M	31.11 ± 1.46	6.06 ± 0.30
BFS/NaOH-14M	26.04 ± 0.79	5.12 ± 0.57
KPH-Ad20-4M	15.31 ± 0.60	3.80 ± 0.35
KPH-Rp20-4M	11.88 ± 0.54	3.41 ± 0.09
OBA-Rp15	16.27 ± 0.72	3.14 ± 0.05
OBA-Rp20	26.01 ± 0.81	6.47 ± 0.55
OBA-Rp25	29.42 ± 1.01	6.30 ± 0.16
OBA-Rp30	31.25 ± 1.00	6.04 ± 0.35
OBA-Rp35	27.81 ± 0.33	5.76 ± 0.16
OBA-Ad5	8.59 ± 0.25	2.64 ± 0.09
OBA-Ad10	16.13 ± 0.22	3.85 ± 0.23
OBA-Ad15	21.47 ± 0.61	3.47 ± 0.47
OBA-Ad20	34.74 ± 1.51	6.88 ± 0.62
OBA-Ad25	38.38 ± 1.29	7.01 ± 0.44

was found for R_f , where the highest strength value of 3.90 MPa was obtained for [KOH] equal to 6 M .

The NaOH series showed similar behaviour to the KOH series. The R_c values increased for [NaOH] = 12 M and decreased for [NaOH] = 14 M . The maximum value was 31.11 MPa , and the lowest was 17.57 MPa . For R_f , the trend was the same, as it increased from 3.95 MPa for [NaOH] = 4 M to 6.05 MPa for [NaOH] = 12 M , and decreased to 5.12 MPa for [NaOH] = 14 M . In general, the strengths for the sodium series were slightly higher than for KOH series. Taking into account the chemical nature of OBA, which was richer in K_2O than in Na_2O , the systems prepared with OBA may be initially compared to those obtained with KOH, although comparisons will be done also to the NaOH series, to assess the equivalency among the ash and the commercial alkaline reagents.

By means of the MIP data on the corresponding pastes (Table 4), it was possible to observe the reduction in the porosity with the increase of the KOH concentration, from 47.16% (P-BFS/KOH-4M) to 23.74% (P-BFS/KOH-8M), as well as the reduction of mean pore

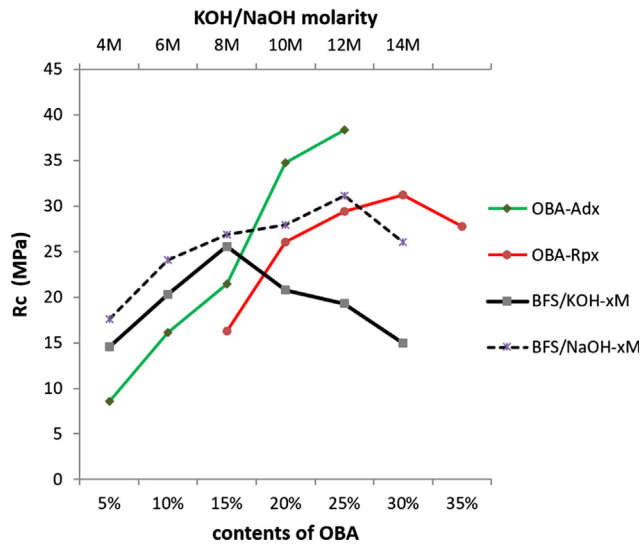


Fig. 5. Compressive strength behaviour of mortars.

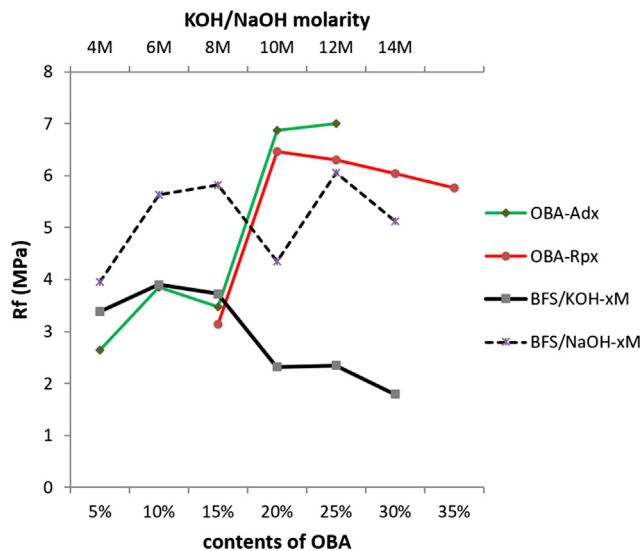


Fig. 6. Flexural strength behaviour of mortars.

diameter (from 48.2 nm to 22.9 nm). These characteristics confirmed the refinement of the pore network, showing the increase in the compactness for P-BFS/KOH-8M, and consequently the higher mechanical strength [46].

Thermal analysis (TG/DTG) for the KOH family registered several mass loss events in the 35–600 °C range (Table 5 and Fig. 7). The first one occurred around 140 °C and indicated the loss of combined water from the main hydrated products, C-S-H and (C,K)-S-H. The second event showed two peaks in the DTG curve at 200 °C and in the 238–259 °C range, which were related to dehydration

of C-A-S-H and (C,K)-A-S-H. The third peak, at about 390 °C, was associated to the presence of hydrocalcite. Similar results were reported by other researchers [8,47,48]. The total mass loss increased with the concentration of KOH, from 12.73% (P-BFS/KOH-4M) to 20.78% (P-BFS/KOH-8M). This indicated that the amount of hydration products in P-BFS/KOH-8M were higher than in P-BFS/KOH-4M. This growth was expected, due to the increase of KOH content available to activate the BFS.

The microstructure of hydrated products is shown in Fig. 8(a) and (b) for P-BFS/KOH-4M, and Fig. 8(c) and (d) for P-BFS/KOH-8M. Both presented a dense matrix with microcrystals and amorphous rounded particles. Microcrystals in P-BFS/KOH-8M were more common, presenting a twinned platelet-like microstructure (Fig. 8(d)). EDS analyses were carried out to compare the composition of the cementing gel in both pastes. Gels analysed in 4 M and 8 M pastes contained similar SiO₂ content (21.6 ± 2.1% vs 23.5 ± 2.3%), Al₂O₃ content (6.8 ± 0.8% vs 7.37 ± 1.4%) and CaO content (28.9 ± 2.1% vs 25.3 ± 7.9%). However, the K₂O content was very different: 33.0 ± 3.6% for 4 M and 27.1 ± 1.7% for 8 M. The higher percentage for the gel formed in 4 M KOH paste suggested that less gel was formed, and the main part of the potassium was incorporated into the hydration products. In this way, a part of the BFS did not react, as suggested by the low value of mass loss in thermogravimetric analysis (Table 5) and the weak strength development (Table 3). In contrast, the higher KOH concentration for the P-BFS/KOH-8M system activated more BFS, producing more hydrates. That is why the potassium content in the formed gel was lower.

3.2. BFS activated by OBA

The effect of OBA on BFS reactivity was assessed by the mechanical strength and microstructure evolution for mortars and pastes produced with different contents of OBA (BFS replacement by OBA or OBA addition to BFS). Table 3 also summarizes the values of Rc and Rf strengths, and Figs. 5 and 6 show the behaviour of the corresponding mortars cured at 65 °C for 7 days.

The replacement series, OBA-Rpz, also showed a nonlinear strength behaviour with replacement percentage (Figs. 5 and 6). Rc increased up to 30% of OBA content (Rc = 31.25 MPa) and decreased for 35% (Rc = 27.81 MPa). The minimum Rc value was found for 5% of OBA content (Rc = 16.27 MPa). A similar trend was described for Rf development, in this case being 20% replacement the optimum (Rf = 6.30 MPa). Despite the lower content in BFS for OBA replacement series, the strength development was good, and strength performance for z = 20–35% was higher than that found for the KOH series. This means that the effectiveness of OBA as an activating reagent largely surpassed KOH. Most likely, the combined effect of potassium and calcium present in OBA makes BFS more reactive. The OBA replacement series had a similar trend to that observed for the NaOH series, and reached strengths that were comparable. Thus, the 12 M NaOH and OBA-Rp30 systems reached optimum strengths (31.11 and 31.25 MPa respectively). Also, 6 M NaOH and OBA-Rp20 were similar. Fittings of compressive strength (Rc, in MPa) versus activation solution

Table 4
Mercury intrusion porosimetry data for P-BFS/KOH-xM and P-OBA-Adx pastes.

Description	Unit	P-BFS/KOH-4M	P-BFS/KOH-8M	P-OBA-Ad10	P-OBA-Ad25
Mean pore diameter	nm	48.20	22.92	16.74	11.87
Volume	cm ³ /g	0.29	0.10	0.20	0.12
Surface area	m ² /g	4.11	6.43	17.42	18.35
Total porosity	%	47.16	23.74	42.85	29.67

Table 5
Thermogravimetric data for selected alkali-activated pastes.

Paste	Mass loss (ML, in %) in the temperature range (°C)			Total mass loss (%)
	0–200 (ML-1)	200–350 (ML-2)	350–600 (ML-3)	
P-BFS/KOH-4M	6.11	4.41	2.21	12.73
P-BFS/KOH-8M	11.78	5	4	20.78
P-KPH-Ad20-4M	3.77	4.01	1.82	9.6
P-OBA-Ad20	5.52	3.3	2.49	11.31
P-OBA-Ad25	8.78	3.47	2.39	14.64

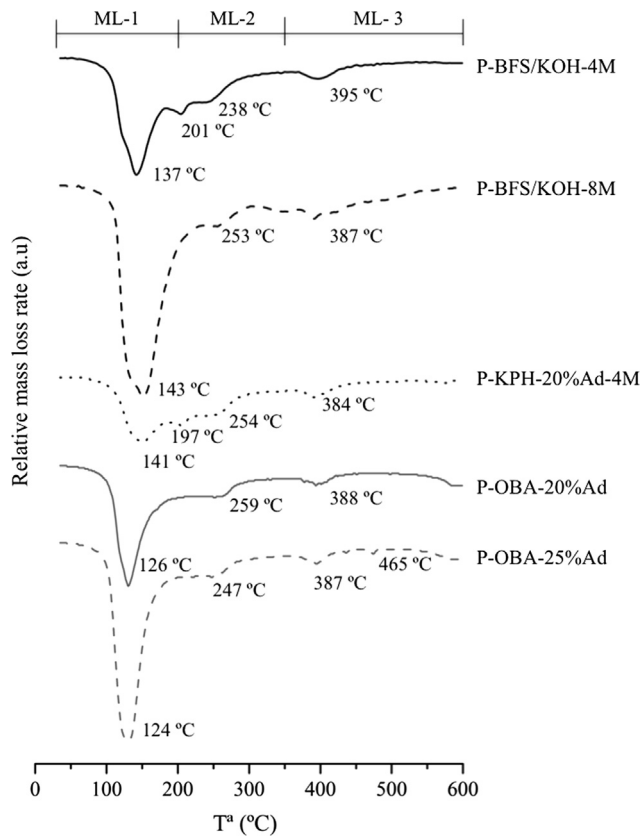


Fig. 7. Selected DTG curves for pastes P-BFS/KOH-4M, P-BFS/KOH-8M, P-KPH-Ad20-4M, P-OBA-Ad20 and P-OBA-Ad25.

parameter (NaOH concentration [NaOH], or OBA replacement [OBA-Rpz]) were calculated as follows by Eqs. (1) and (2):

$$Rc = 11.592 * \ln[\text{NaOH}] + 2.201 \quad (1)$$

$$Rc = 21.577 * \ln[\text{OBA} - \text{Rpz}] - 40.741 \quad (2)$$

From these equations, a relationship for the equivalency between NaOH concentration and OBA replacement can be calculated (Fig. 9).

The addition series (BFS content was maintained constant and OBA was added in different percentages with respect to BFS), OBA-Ady, showed a continuously increasing strength up to 25% content of OBA (Figs. 5 and 6). The maximum values for Rc and Rf were found with 25% of OBA (Rc = 38.38 MPa and Rf = 7.01 MPa), and the minimum values were found with 5% of OBA (Rc = 8.59 MPa and Rf = 2.64 MPa). Compressive strength depended linearly on the OBA addition (OBA-Ady), as shown in Eq. (3):

$$Rc = 1.564 * [\text{OBA} - \text{Ady}] + 0.405 \quad (3)$$

Equivalency analysis for compressive strength revealed that Rc values using NaOH solutions (range from 17.57 to 31.11 MPa) were reached by using OBA addition percentages between 10.97% and

19.63%, according to Eq. (3). The higher OBA addition percentage produced better mortars in terms of strength. Based on the reference family mortars activated with KOH and NaOH, it is clear that mortars produced with the addition of OBA, in amounts of 20% and 25%, presented compressive strength values higher than those developed by the reference series, which reached their maximums in 8 M for KOH (Rc = 25.56 MPa), and in 12 M for NaOH (Rc = 31.11 MPa).

The results of MIP tests (Table 4) showed a significant reduction of porosity and mean pore diameter with the increase of OBA contents from 10 to 25%. Thus, P-OBA-Ad10 paste had 42.85% total porosity and P-OBA-Ad25 had 29.67%. This explained the large differences in strength (16.13 MPa vs. 38.38 MPa). Also, the lowest mean pore diameter value was found for P-OBA-Ad25 (11.9 nm). This means that the microstructure of the activated material became more refined with increasing OBA addition, justifying the increase of mechanical strengths in the corresponding mortars.

Comparing the series P-BFS/KOH-x with P-OBA-Ady, a significant change in the total porosity was not observed (P-BFS/KOH-8M vs. P-OBA-Ad25, 23.74% vs 29.67%). However, the mechanical strengths of the corresponding mortars showed strong differences: BFS/KOH-8 M (Rc = 25.56 MPa, Rf = 5.81 MPa) and OBA-Ad25 (Rc = 38.38 MPa, Rf = 7.01 MPa).

The gain in strength for the OBA series could be attributed to the nature of the hydrated products. Also, the filler effect of the OBA may be taken into account: OBA was not dissolved totally in water, and consequently a filler effect (more fine particles in the mortar matrix) could play an additional role.

3.2.1. Analysis of the filler effect

The filler effect of the OBA was assessed considering the behaviour of the mechanical strengths of mortars produced with an inert material. Kephallite (KPH, andalucite) presented a similar fineness to OBA (Fig. 2). Two types of mortars, KPH-Ad20-4M (addition of 20% KPH by mass respect to BFS content, and activated with 4 M KOH solution) and KPH-Rp20-4M (replacement of 20% BFS by KPH, and activated with 4 M KOH solution), were tested. The strength values are summarized in Table 3 and the behaviour depicted in Fig. 10. They were analysed the values for: a) replacement (BFS/KOH-4M, KPH-Rp20-4M, OBA-Rp20) and b) addition (BFS/KOH-4M, KPH-Ad20-4M, OBA-Ad-20). The replacement series showed that the inert-containing mortar yielded 11.88 MPa, which is slightly lower than the corresponding BFS/KOH sample ($\approx 18\%$ less strength). This means that KPH contributed as an inert material. The addition series showed that inert-containing mortar yielded 15.31 MPa, slightly higher than the corresponding BFS/KOH sample ($\approx 5\%$). This behaviour suggests that, despite having the same BFS content and a larger quantity of fine particles, the filler contribution to strength development was practically negligible. Considering the filler effect as a function of the fineness (PDS), and the similarity of PDS curves for KPH and OBA (Fig. 2), it is suggested that the filler effect did not contribute significantly to the strength gain of the mortars produced with the OBA. The large strength gain observed when comparing the KOH activated sample and OBA activated sample in the replacing ($\approx 79\%$ gain)

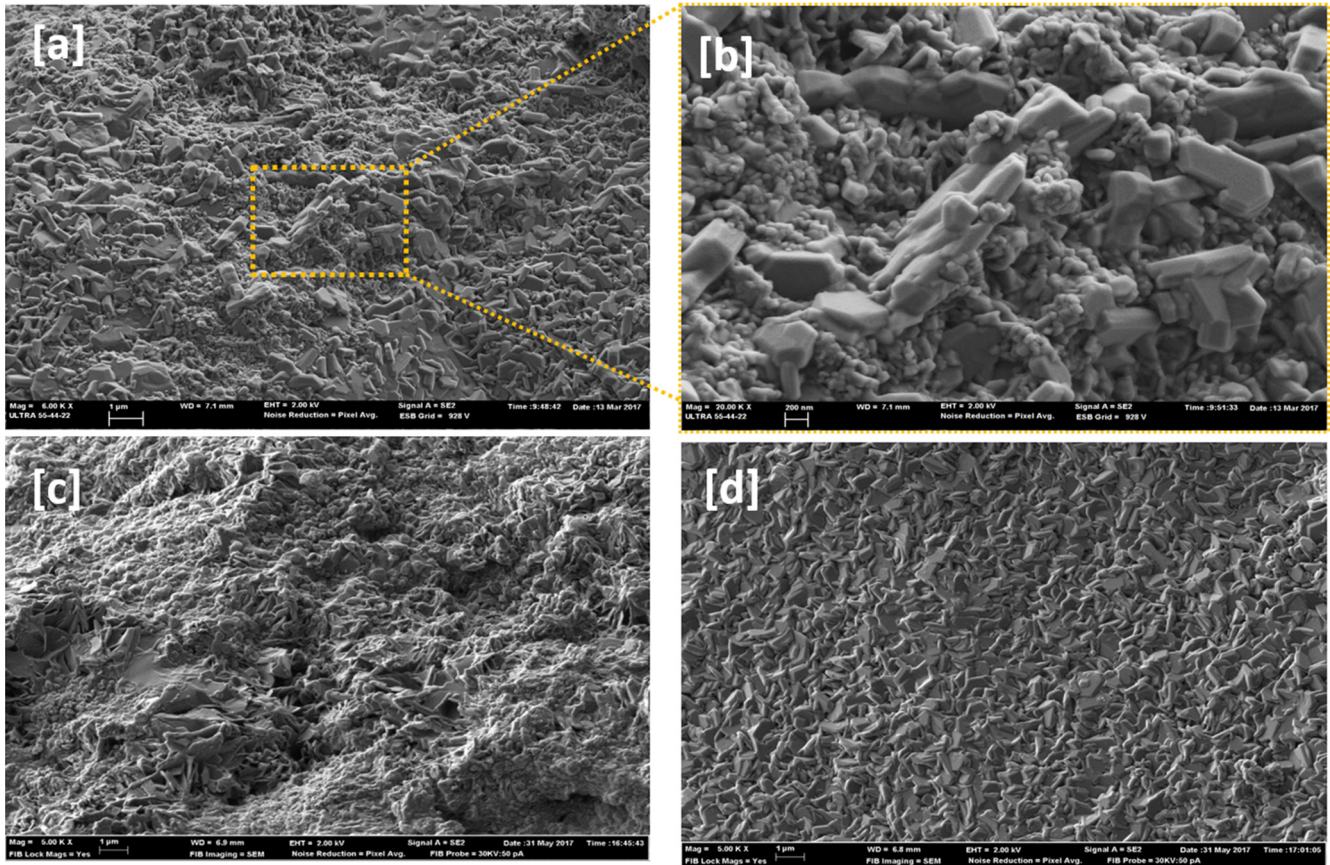


Fig. 8. FESEM micrographs of BFS pastes activated with KOH solution: a) General view for P-BFS/KOH-4M matrix; b) Detail from the above micrograph; c) General view for P-BFS/KOH-8M; d) microcrystals in P-BFS/KOH-8M.

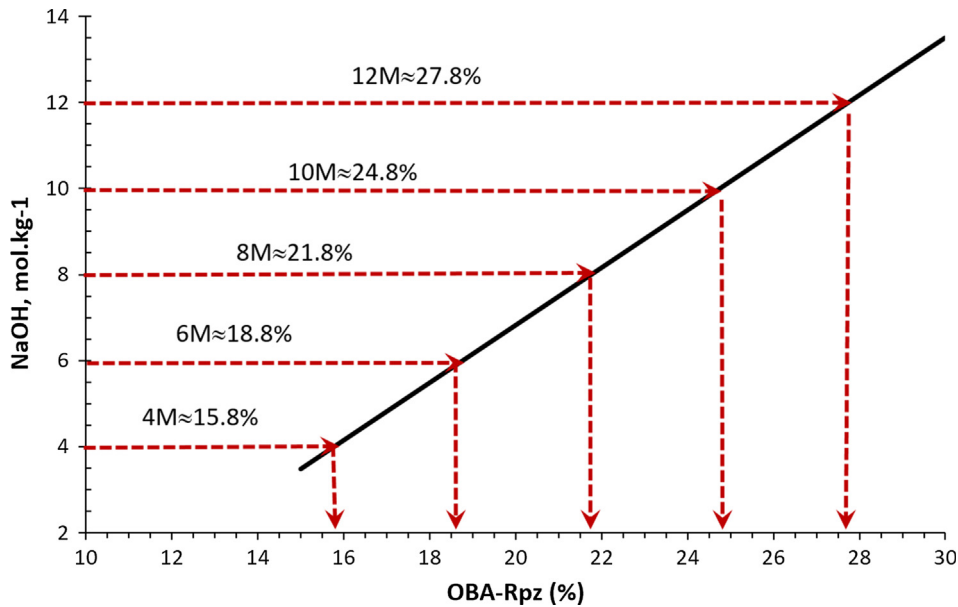


Fig. 9. Equivalences between the NaOH concentration and % of OBA replacement, in BFS mortars.

and addition ($\approx 138\%$ gain) tests is attributed to the contribution of OBA to the hydration of BFS.

3.2.2. Hydration products in BFS/OBA activated systems

TG/DTG results for KPH and OBA pastes are shown in Fig. 7 and Table 5. The total mass loss for P-KPH-Ad20-4M was lower ($\approx 25\%$)

than that found for P-BFS/KOH-4M, which was attributed to the dilution effect produced with the addition of the inert material. The temperature DTG peaks were very similar, when comparing curves in Fig. 7.

DTG curves for OBA containing pastes showed a large peak at $124\text{--}126\text{ }^\circ\text{C}$, which indicated that the nature and amount of

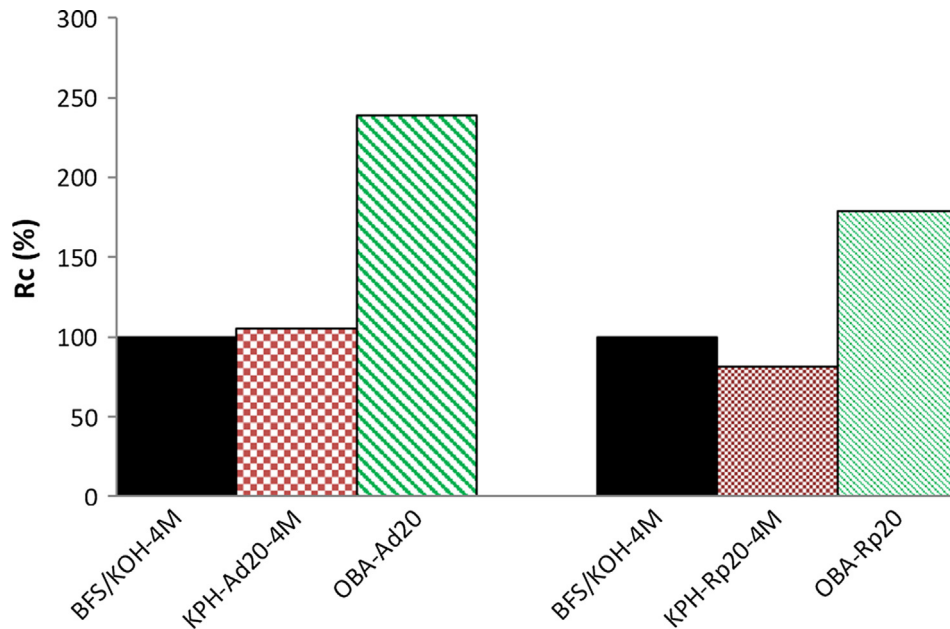


Fig. 10. Filler effect assessment from compressive strength values.

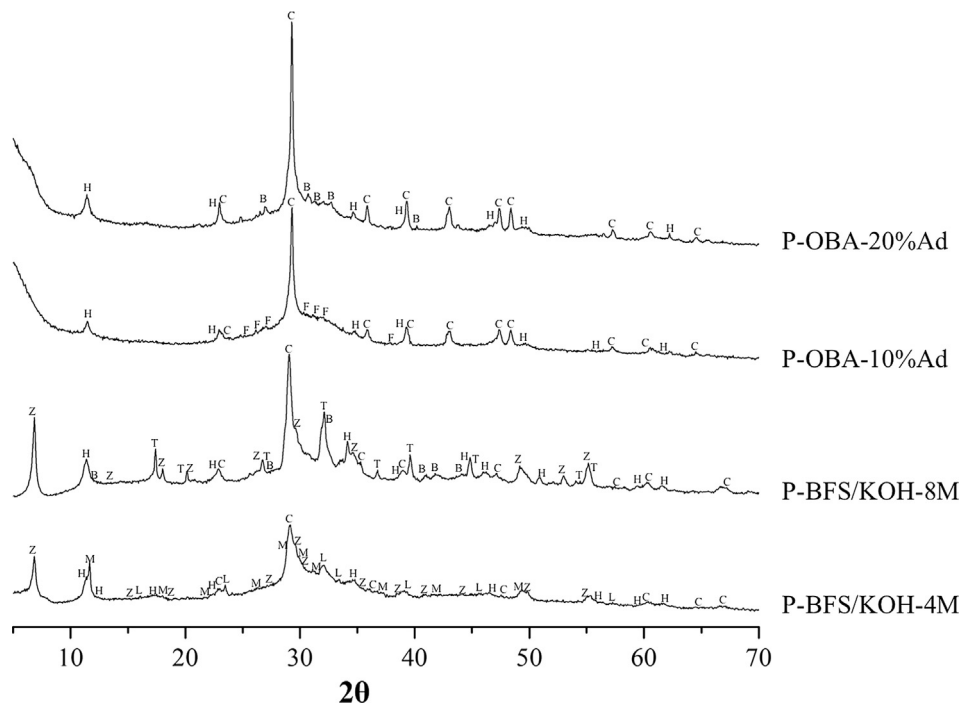


Fig. 11. X-ray diffraction patterns for P-BFS/KOH-4M, P-BFS/KOH-8M, P-OBA-Ad10 and P-OBA-Ad25 (Key: C, calcite; Z, zeolite K-I, H, hydrotalcite; M, potassium gismondine; L, larnite; T, katoite; B, potassium carbonate hydrate; F, fukalite).

hydrates were slightly different than those observed in the KOH activated BFS-pastes. However, the total mass loss (Table 5) for the OBA containing pastes was significantly lower than that found for KOH pastes. For example, P-BFS/KOH-8M showed 20.73% total mass loss, while P-OBA-Ad25 had only 14.71%. This behaviour suggests that despite the lower amount of combined water, the mechanical properties and chemical nature of the hydrates formed in the activation of BFS in the presence of OBA is different than expected.

Results from XRD analyses on selected pastes are shown in Fig. 11. The differences between KOH and OBA activated pastes

are clear. Both BFS pastes activated with KOH (4 M and 8 M) showed calcite, hydrotalcite ($Mg_6Al_2CO_3(OH)_{16} \cdot 4H_2O$, PDF card 140191) and K-I zeolite ($K_2Al_2Si_2O_8 \cdot 3.8H_2O$, PDF card 180988) as main crystalline products. Most likely, the calcite presence was because it was in the BFS composition; the rest of products were formed from the hydration processes. Additional zeolitic phases were formed in these KOH pastes. Potassium gismondine ($K_2A_2ISi_2O_8 \cdot 3H_2O$, PDF card 110188) was identified in the XRD pattern of 4 M KOH activated paste and katoite ($Ca_3Al_2(SiO_4)(OH)_8$, PDF card 380368) was identified for the 8 M activated paste. Also, in this last paste, potassium carbonate hydrate ($K_2CO_3 \cdot 1.5H_2O$, PDF

card 110655) was found, and its presence may be due to the carbonation of unreacted KOH.

OBA containing pastes (10 and 25% addition of OBA to BFS) also showed calcite as the main crystalline product in the XRD patterns, due to the presence of this phase in BFS and in OBA. However, the main crystalline compound formed under the activation by OBA was hydrocalcite. No presence of katoite and K-I zeolite was observed suggesting that evolution of zeolitic structures were not developed. This behaviour is in agreement with the better mechanical strength found for OBA containing systems. In the 10% and 25% OBA pastes, small amounts of fukalite ($\text{Ca}_4\text{Si}_2\text{O}_6(\text{CO}_3)(\text{OH})_2$, PDF card 290308) and potassium carbonate hydrate, respectively, were found.

The microstructure of the hydrated products in pastes was analysed by FESEM in Fig. 12 (P-OBA-Ad10) and Fig. 13 (P-OBA-Ad25). P-OBA-Ad25 presented a more compact microstructure than P-OBA-Ad10, and their microstructures were slightly different from the reference pastes (P-BFS/KOH-xM, see Fig. 8). Two different gels were observed in pastes with OBA: a dense one and a compact one. The morphology of the microcrystals (denser phases) was different that that observed for reference pastes, suggesting that these differences may be responsible of the different mechanical behaviour of the corresponding mortars.

The mean chemical composition values were obtained by averaging 8–10 EDS data sets (see Table 6). The SiO_2 content in OBA containing pastes (29.17 ± 3.39 for 10% OBA, 28.91 ± 1.61 for 25% OBA) was significantly higher than those found for KOH activated pastes. The same behaviour was found for Al_2O_3 and CaO contents.

The CaO content was significantly high, reaching values from 34 to 41%, suggesting that calcium from OBA also reacted with the BFS. The K_2O content was significantly lower, ranging less than a half of the percentage found in KOH activated pastes. All these differences indicated that the activation of BFS was more complete in the presence of OBA.

4. Conclusions

The ash obtained from the combustion of olive-stone biomass (OBA) was tested as an activator reagent for blast furnace slag (BFS), and compared to the effect of typical activating solutions of KOH and NaOH (in the range 4–14 mol·kg⁻¹). The chemical composition of OBA showed high percentages of K_2O and CaO, which become interesting for preparing BFS activated systems. The effect of OBA on the strength development of BFS-based mortars was very significant for both partial replacement of BFS and addition to BFS. The compressive strength of mortars with 20–35% replacement of BFS by OBA yielded higher values than those obtained for BFS-KOH systems. An equivalency between NaOH concentration in the activating solution and OBA replacement in the activation of BFS was found (e.g., 4 M NaOH was equivalent to 15.8% OBA replacement and 8 M NaOH to 27.8% OBA replacement). The addition of 25% of OBA enabled reaching a value of 38 MPa in compressive strength. The effect of OBA on the microstructure was studied, and the main features to highlight were the reduction in the mean pore diameter in the BFS activated paste and the very limited formation of zeolitic phases.

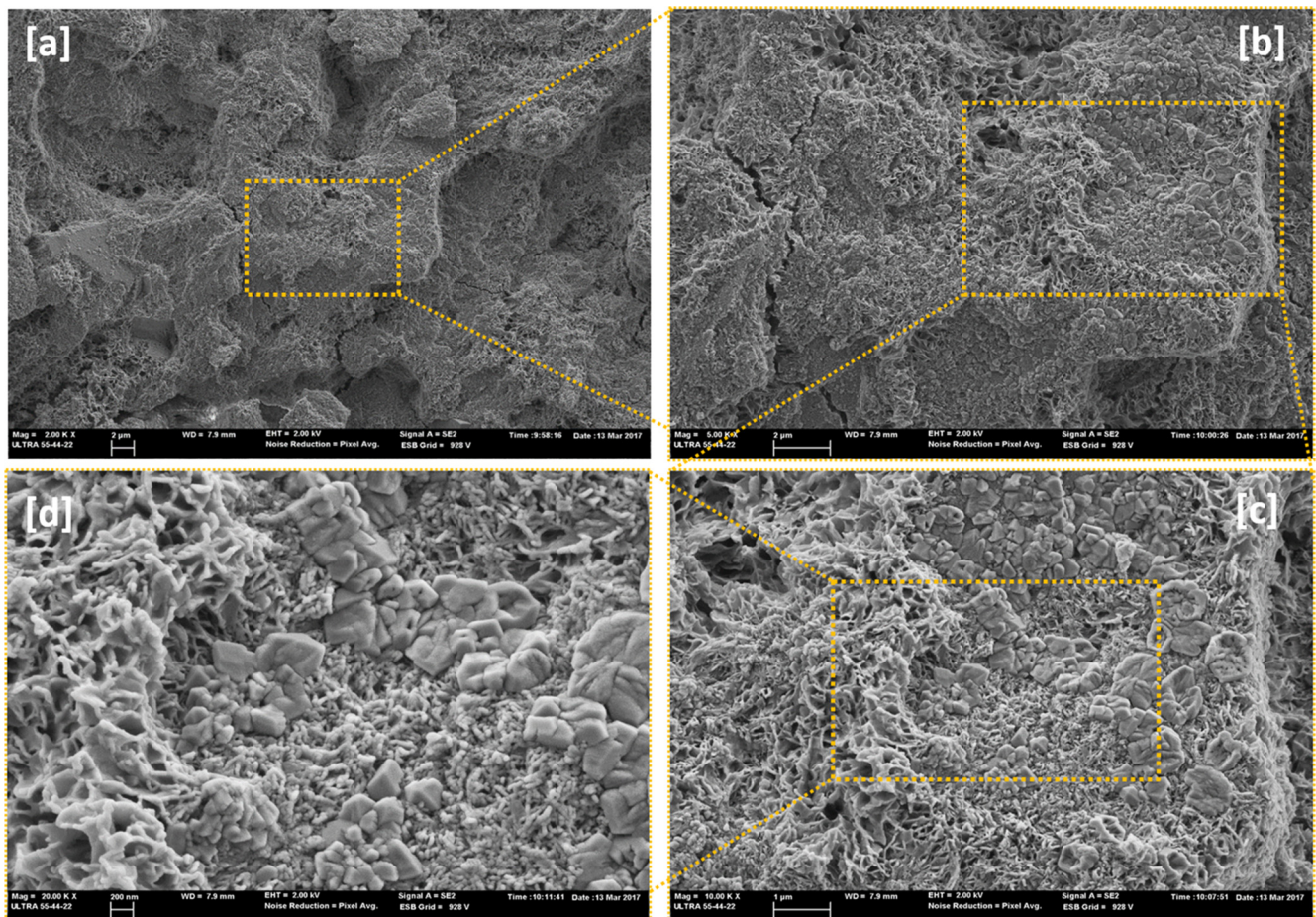


Fig. 12. FESEM micrographs of BFS pastes activated with 10% OBA (P-OBA-Ad10): a) general view, b) detail from the above micrograph, c) magnification of the above one, showing porous and dense particles and d) detailed view of the nature of the different formed gels.

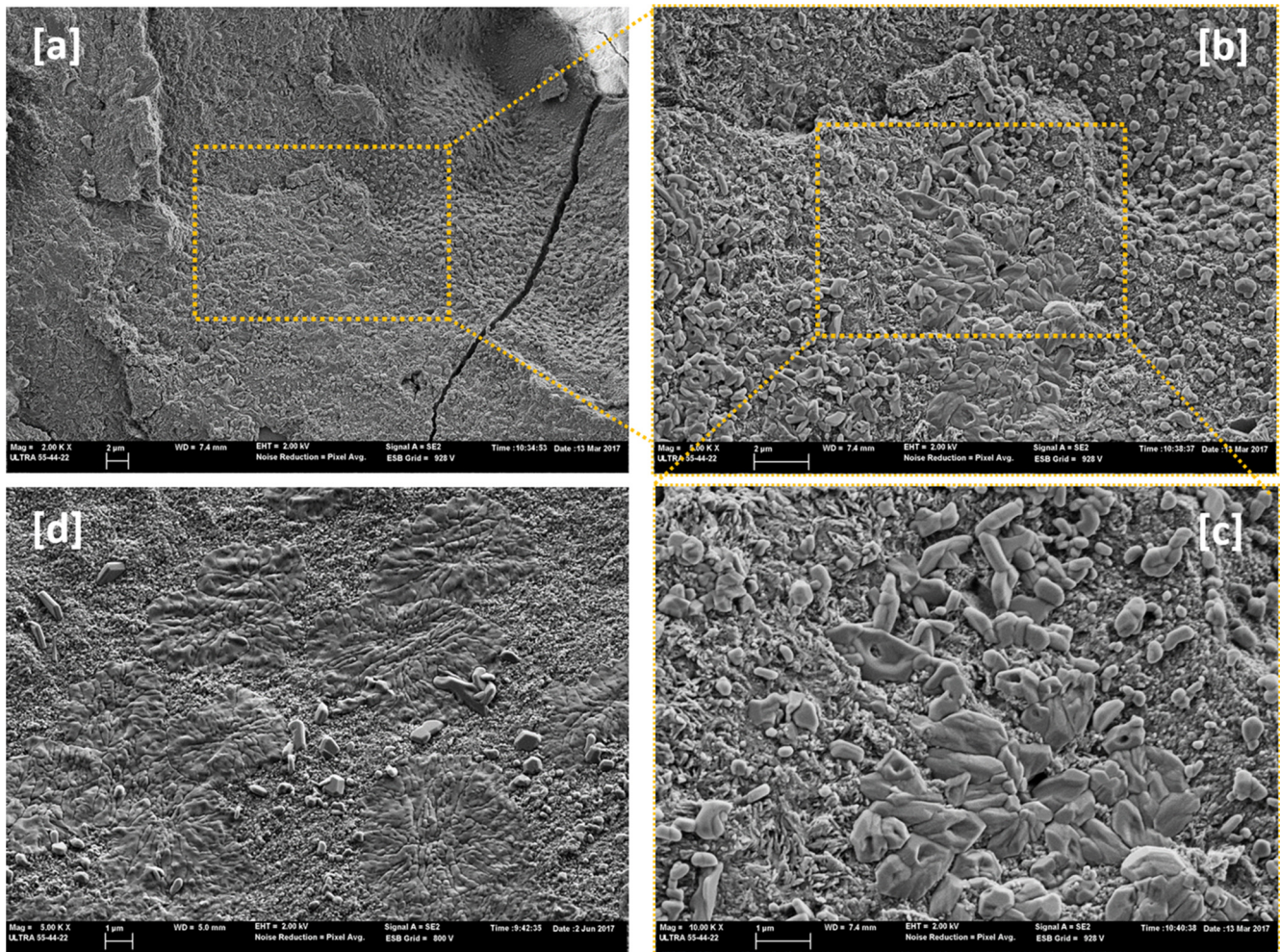


Fig. 13. FESEM micrographs of BFS pastes activated with 25% OBA (P-OBA-Ad25): a) general view, b) detail from the above micrograph, c) magnification of the above one, showing porous and dense particles and d) another view of the two types of gel.

Table 6

Chemical composition (EDS analysis) for studied pastes.

Oxide (% by mass)	P-BFS/KOH-4M	P-BFS/KOH-8M	P-OBA-Ad10%	P-OBA-Ad25%
Na ₂ O	2.45 ± 0.59	1.64 ± 1.07	0.18 ± 0.37	0.60 ± 0.42
MgO	3.39 ± 0.79	4.15 ± 1.22	5.27 ± 0.64	7.47 ± 1.38
Al ₂ O ₃	6.76 ± 0.80	7.37 ± 1.41	8.73 ± 1.09	9.61 ± 1.11
SiO ₂	21.61 ± 2.14	23.50 ± 2.35	29.17 ± 3.39	28.91 ± 1.61
SO ₃	0.92 ± 1.14	5.27 ± 2.45	3.93 ± 1.20	4.07 ± 1.28
K ₂ O	32.99 ± 3.64	27.16 ± 1.70	11.23 ± 2.64	14.91 ± 3.27
CaO	28.94 ± 2.08	25.28 ± 7.93	41.19 ± 3.03	34.04 ± 1.54

This study demonstrated the viability of using OBA in the activation of BFS and the reduction in the consumption of commercial chemical reagents for AAM preparation. This allows a more sustainable AAM.

Conflict of interest

None.

Acknowledgements

The authors are grateful to CAPES for the scholarship. Thanks are also given to Electron Microscopy Service of the Universitat

Politécnica de València, the GeocelPlus-UPV project and Almazara Candela – Elche, Spain.

References

- [1] L.K. Turner, F.G. Collins, Carbon dioxide equivalent (CO₂-e) emissions: a comparison between geopolymer and OPC cement concrete, *Constr. Build. Mater.* 43 (2013) 125–130, <https://doi.org/10.1016/j.conbuildmat.2013.01.023>.
- [2] F. Pacheco-Torgal, J. Labrincha, C. Leonelli, A. Palomo, P. Chindaprasit, *Handbook of Alkali-Activated Cements, Mortars and Concretes*, Woodhead Publishing – Elsevier, 2014.
- [3] J. Davidovits, *Geopolymer Chemistry and Application*, fourth ed., Institut Géopolymère, France, 2015.
- [4] A. Palomo, P. Krivenko, I. Garcia-Lodeiro, E. Kavalerova, O. Maltseva, A. Fernández-Jiménez, A review on alkaline activation: new analytical

- perspectives, *Mater. Constr.* 64 (2014) e022, <https://doi.org/10.3989/mc.2014.00314>.
- [5] A. Fernández-Jiménez, F. Puertas, Influence of the activator concentration on the kinetics of the alkaline activation process of a blast furnace slag, *Mater. Constr.* 47 (1997) 31–42.
- [6] A. Fernández-Jiménez, J.G. Palomo, F. Puertas, Alkali-activated slag mortars: mechanical strength behaviour, *Cem. Concr. Res.* 29 (1999) 1313–1321, [https://doi.org/10.1016/S0008-8846\(99\)00154-4](https://doi.org/10.1016/S0008-8846(99)00154-4).
- [7] F. Pelisser, E.L. Guerrino, M. Menger, M.D. Michel, J.A. Labrincha, Micromechanical characterization of metakaolin-based geopolymers, *Constr. Build. Mater.* 49 (2013) 547–553, <https://doi.org/10.1016/j.conbuildmat.2013.08.081>.
- [8] U. Rattanasak, P. Chindaprasirt, Influence of NaOH solution on the synthesis of fly ash geopolymer, *Miner. Eng.* 22 (2009) 1073–1078, <https://doi.org/10.1016/j.mineng.2009.03.022>.
- [9] J. Temuujin, A. Riessen, K.J.D. MacKenzie, Preparation and characterisation of fly ash based geopolymer mortars, *Constr. Build. Mater.* 24 (2010) 1906–1910, <https://doi.org/10.1016/j.conbuildmat.2010.04.012>.
- [10] M.M. Tashima, J.L. Akasaki, V.N. Castaldelli, L. Soriano, J. Monzó, J. Payá, M.V. Borrachero, New geopolymeric binder based on fluid catalytic cracking catalyst residue (FCC), *Mater. Lett.* 80 (2012) 50–52, <https://doi.org/10.1016/j.matlet.2012.04.051>.
- [11] L. Reig, M.M. Tashima, M.V. Borrachero, J. Monzó, C.R. Cheeseman, J. Payá, Properties and microstructure of alkali-activated red clay brick waste, *Constr. Build. Mater.* 43 (2013) 98–106, <https://doi.org/10.1016/j.conbuildmat.2013.01.031>.
- [12] R.H. Geraldo, C.M. Ouellet-Plamondon, E.A.D. Muianga, G. Camarini, Alkali-activated binder containing wastes: a study with rice husk ash and red ceramic, *Cerâmica* 63 (2017) 44–51, <https://doi.org/10.1590/0366-69132017633652057>.
- [13] R.A.A.B. Santa, A.M. Bernardin, Geopolymer synthesized from bottom coal ash and calcined paper sludge, *J. Clean. Prod.* 57 (2013) 302–307, <https://doi.org/10.1016/j.jclepro.2013.05.017>.
- [14] J.C.B. Moraes, M.M. Tashima, J.L. Akasaki, J.L.P. Melges, J. Monzó, M.V. Borrachero, L. Soriano, J. Payá, Increasing the sustainability of alkali-activated binders: the use of sugar cane straw ash (SCSA), *Constr. Build. Mater.* 124 (2016) 148–154, <https://doi.org/10.1016/j.conbuildmat.2016.07.090>.
- [15] X. Gao, Q.L. Yu, A. Lazaro, H.J.H. Brouwers, Investigation on a green olivine nano-silica source based activator in alkali activated slag-fly ash blends: reaction kinetics, gel structure and carbon footprint, *Cem. Concr. Res.* 100 (2017) 129–139, <https://doi.org/10.1016/j.cemconres.2017.06.007>.
- [16] A. Mellado, C. Catalán, N. Bouzón, M.V. Borrachero, J. Monzó, J. Payá, Carbon footprint of geopolymeric mortar: study of the contribution of the alkaline activating solution and assessment of an alternative route, *RSC Adv.* 4 (2014) 23846–23852, <https://doi.org/10.1039/c4ra03375b>.
- [17] J.M. Mejía, R. Mejía de Gutiérrez, F. Puertas, Rice husk ash as a source of silica in alkali-activated fly ash and granulated blast furnace slag systems, *Mater. Constr.* 63 (2013) 361–375, <https://doi.org/10.3989/mc.2013.04712>.
- [18] N. Bouzón, J. Payá, M.V. Borrachero, L. Soriano, M.M. Tashima, J. Monzó, Refluxed rice husk ash/NaOH suspension for preparing alkali activated binders, *Mater. Lett.* 115 (2014) 72–74, <https://doi.org/10.1016/j.matlet.2013.10.001>.
- [19] R.H. Geraldo, L.F.R. Fernandes, G. Camarini, Water treatment sludge and rice husk ash to sustainable geopolymer production, *J. Clean. Prod.* 149 (2017) 146–155, <https://doi.org/10.1016/j.jclepro.2017.02.076>.
- [20] J.M. Mejía, R. Mejía de Gutiérrez, C. Montes, Rice husk ash and diatomaceous earth as a source of silica to fabricate a geopolymeric binary binder, *J. Clean. Prod.* 118 (2016) 33–139, <https://doi.org/10.1016/j.jclepro.2016.01.057>.
- [21] A. Fernández-Jiménez, N. Cristelo, T. Miranda, A. Palomo, Sustainable alkali activated materials: precursor and activator derived from industrial wastes, *J. Clean. Prod.* 162 (2017) 1200–1209, <https://doi.org/10.1016/j.jclepro.2017.06.151>.
- [22] A. Font, L. Soriano, J.C.B. Moraes, M.M. Tashima, J. Monzó, M.V. Borrachero, J. Payá, A 100% waste-based alkali-activated material by using olive-stone biomass ash (OBA) and blast furnace slag (BFS), *Mater. Lett.* 203 (2017) 46–49, <https://doi.org/10.1016/j.matlet.2017.05.129>.
- [23] A. Peys, H. Rahier, Y. Pontikes, Potassium-rich biomass ashes as activators in metakaolin-based inorganic polymers, *Appl. Clay Sci.* 119 (2016) 401–409, <https://doi.org/10.1016/j.clay.2015.11.003>.
- [24] A. Roig, M.L. Cayuela, M.A. Sánchez-Monedero, An overview on olive mill wastes and their valorisation methods, *Waste Manage.* 26 (2006) 960–969, <https://doi.org/10.1016/j.wasman.2005.07.024>.
- [25] Junta de Andalucía, Potencial energético de los subproductos de la industria olivarera en Andalucía, Secretaría General del Medio Rural y la Producción Ecológica, 2010. http://ws128.juntadeandalucia.es/agriculturaypesca/portal/export/sites/default/comun/galerias/galeriaDescargas/cap/servicio-estadisticas/Estudios-e-informes/desarrollo-rural-sost/IND_OLIVAR_V1_CC.pdf.
- [26] E. Romero, M. Quirantes, R. Nogales, Characterization of biomass ashes produced at different temperatures from olive-oil-industry and greenhouse vegetable wastes, *Fuel* 208 (2017) 1–9, <https://doi.org/10.1016/j.fuel.2017.06.133>.
- [27] R.M.L. Medeiros, F. Villa, D.F. Silva, L.R.C. Júlio, Destinação e reaproveitamento de subprodutos da extração olivícola, *Sci. Agrar. Parana.* 15 (2016) 100–108, <https://doi.org/10.18188/1983-1471/sap.v15n2p100-108> (in Portuguese).
- [28] A.G. Vlyssides, M. Loizides, P.K. Karlis, Integrated strategic approach for reusing olive oil extraction by-products, *J. Clean. Prod.* 12 (2004) 603–611, [https://doi.org/10.1016/S0959-6526\(03\)00078-7](https://doi.org/10.1016/S0959-6526(03)00078-7).
- [29] S. Souilem, A. El-Abbassi, H. Kiai, A. Hafidi, S. Sayadi, C.M. Galanakis, Olive oil production sector environmental effects and sustainability challenges, in: C.M. Galanakis (Ed.), *Olive Mill Waste: Recent Advance for Sustainable Management*, 2017, <https://doi.org/10.1016/B978-0-12-805314-0-00001-7>.
- [30] J.A. Albuquerque, J. González, D. García, J. Cegarra, Agrochemical characterisation of ‘alperujo’, a solid by-product of the two-phase centrifugation method for olive oil extraction, *Bioresour. Technol.* 91 (2004) 195–200, [https://doi.org/10.1016/S0960-8524\(03\)00177-9](https://doi.org/10.1016/S0960-8524(03)00177-9).
- [31] A.E. Hanandeh, Energy recovery alternatives for the sustainable management of olive oil industry waste in Australia: life cycle assessment, *J. Clean. Prod.* 91 (2015) 78–88, <https://doi.org/10.1016/j.jclepro.2014.12.005>.
- [32] A.C. Caputo, F. Scacchia, P.M. Pelagagge, Disposal of by-products in olive oil industry: waste-to-energy solutions, *Appl. Therm. Eng.* 23 (2003) 197–214, [https://doi.org/10.1016/S1359-4311\(02\)00173-4](https://doi.org/10.1016/S1359-4311(02)00173-4).
- [33] N.G. Nair, J. Markham, Recycling Solid Waste from the Olive Oil Extraction, Rural Industries Research and Development Corporation – Australian Government, 2008. <https://rirdc.infoservices.com.au/downloads/08-16>.
- [34] IOC-International Olive Oil Council, 2017, World Olive Oil Figures. (http://www.internationaloliveoil.org/estaticos/view/131-world-olive-oil-figures?lang=en_US).
- [35] D. Vamvuka, D. Zografos, Predicting the behaviour of ash from agricultural wastes during combustion, *Fuel* 83 (2004) 2051–2057, <https://doi.org/10.1016/j.fuel.2004.04.012>.
- [36] N.M. Al-Akhras, K.M. Al-Akhras, M.F. Attom, Performance of olive waste ash concrete exposed to elevated temperatures, *Fire Saf. J.* 44 (2009) 370–375, <https://doi.org/10.1016/j.firesaf.2008.08.006>.
- [37] N.M. Al-Akhras, M.Y. Abdulwahid, Utilisation of olive waste ash in mortar mixes, *Struct. Concr.* 11 (2010) 221–228, <https://doi.org/10.1680/stco.2010.11.4.221>.
- [38] N.M. Al-Akhras, Performance of olive waste ash concrete exposed to alkali-silica reaction, *Struct. Concr.* 13 (2012) 221–226, <https://doi.org/10.1002/suco.201100058>.
- [39] A. Eisa, Properties of concrete incorporating recycled post-consumer environmental wastes, *Int. J. Concr. Struct. Mater.* 8 (2014) 251–258, <https://doi.org/10.1007/s40069-013-0065-9>.
- [40] M. Cruz-Yusta, J. Morales Mármol, L. Sánchez, Use of olive biomass fly ash in the preparation of environmentally friendly mortars, *Environ. Sci. Technol.* 45 (2011) 6991–6996, <https://doi.org/10.1021/es200968a>.
- [41] S.V. Vassilev, D. Baxter, L.K. Andersen, C.G. Vassileva, An overview of the chemical composition of biomass, *Fuel* 89 (2010) 913–933, <https://doi.org/10.1016/j.fuel.2009.10.022>.
- [42] J. Cuenca, J. Rodríguez, M. Martín-Morales, Z. Sánchez-Roldán, M. Zamorano, Effects of olive residue biomass fly ash as filler in self-compacting concrete, *Constr. Build. Mater.* 40 (2013) 702–709, <https://doi.org/10.1016/j.conbuildmat.2012.09.101>.
- [43] A. Demirbas, Combustion characteristics of different biomass fuels, *Prog. Energy Combust. Sci.* 30 (2004) 219–230, <https://doi.org/10.1016/j.pecs.2003.10.004>.
- [44] P.E. Miles, Alkali Deposits Found in Biomass Power Plants – A Preliminary Investigation of Their Extent and Nature, National Renewable Energy Laboratory (Colorado, USA), 1995. <https://www.nrel.gov/docs/legosti/fy96/8142v1.pdf>.
- [45] UNE-EN 196-1, Methods of Testing Cement – Part 1: Determination of Strength, AENOR, 2005.
- [46] X. Chen, S. Wu, J. Zhou, Influence of porosity on compressive and tensile strength of cement mortar, *Constr. Build. Mater.* 40 (2013) 869–874, <https://doi.org/10.1016/j.conbuildmat.2012.11.072>.
- [47] A.A. Abdel-Gawwad, S. Abd El-Aleem, Effect of reactive magnesium on properties of alkali activated slag cement pastes, *Ceramics – Silikáty* 59 (2015) 37–47, [https://doi.org/10.1061/\(ASCE\)MT.1943-5533.0001207](https://doi.org/10.1061/(ASCE)MT.1943-5533.0001207).
- [48] O.G. Rivera, W.R. Long, C.A. Weiss Jr., R.D. Moser, B.A. Williams, K. Torres-Cancel, E.R. Gore, P.G. Allison, Effect of elevated temperature on alkaliactivated geopolymeric binders compared to Portland cement-based binders, *Cem. Concr. Res.* 90 (2016) 43–51, <https://doi.org/10.1016/j.cemconres.2016.09.013>.